ORIGINAL ARTICLE

Increasing formability in hole-flanging through the use of punch rotation based on temperature and strain rate dependent forming limit curves

Lemopi Isidore Besong[1] · Johannes Buhl[1] · Markus Bambach[1,2]

Abstract

Conventional hole-flanging by stamping is characterized by low formability. It is common knowledge that formability can be improved by forming at high temperatures. High-speed punch rotation is introduced to conventional hole-flanging to use frictional heat to improve and control formability. Thermomechanical finite element (FE) simulations of conventional hole-flanging and hole-flanging with punch rotation are used to determine the effects of punch rotation on the process temperature. Hot tensile tests were conducted to find the effects of temperature and strain rate on the forming limit of the blank. The Marciniak–Kuczynski (M–K) forming limit model is used to estimate temperature and strain-rate dependent forming limits of the material. Hole flanging experiments were conducted at different punch speeds and feeds to determine process windows that maximize formability. A maximum hole expansion ratio (HER) of 4 was obtained in hole-flanging with punch rotation compared to 1.48 in conventional hole-flanging experiments. In theory, a rise in blank temperature to 400 °C in hole-flanging with punch rotation enhances the HER by 30% based on the FE simulations. However, experiments of hole-flanging with punch rotation reveal a 170% increase in formability. The difference in formability between the experiments and FE simulations is attributed to the influence of high-speed deformation, in-plane shear and non-proportional loading paths. To control formability in hole-flanging with high-speed punch rotation, it seems sufficient to establish a closed-loop control of the process with a pre-defined temperature profile.

Keywords Hole-flanging · Frictional heating · High formability · High-speed forming · Process control

Introduction

Hole-flanging is a sheet metal forming process used to form flanges (collars) around holes in sheet metals. Traditionally, flanges are made by stamping operations. Blanks with pre-cut holes are clamped using a die and blank holder, while a punch expands the holes to flanges. The blanks are bent to the desired angle (usually 90°). Flanges may be classified into convex, concave, and straight flanges based on their shape. Flanges serve as connector elements between tubes and sheet parts in assemblies, fluid passages, and provide holes needed for threading operations.

Because of the importance of flanges in metalworking, several studies have been undertaken to determine the process mechanics and find the forming limits in hole-flanging by stamping. Using FE simulations, Worswick and Finn [1] showed that deformation at the flange edge occurs by uniaxial tension since the blank is deformed by stretching along the circumferential axis and shortening along the meridional and radial axes. The maximum deformation of the blank occurs at the flange edge and deformation reduces towards the clamped end. Suzuki et al. [2] analyzed the effect of sheet anisotropy on the HER of flanges using experimental investigations and FE analyzes. They concluded that the HER of flanges highly depends on the anisotropy of the blanks. Cracks occurred in the regions of the flange edge with the lowest tensile strength. Yoon et al. [3] showed that hole-flange ability can be estimated using the fracture toughness of the blank material. Fracture toughness tests

✉ Lemopi Isidore Besong
  besonlem@b-tu.de

1 Chair of Mechanical Design and Manufacturing, Brandenburg University of Technology, Cottbus - Senftenberg, Konrad - Wachsmann - Allee 17, 03046 Cottbus, Germany

2 Advanced Manufacturing Lab, ETH Zurich, Leonhardstrasse 27, 8092 Zurich, Switzerland

and hole-flanging experiments conducted on 8 materials with different microstructures were used to arrive at this conclusion.

The forming limit of hole-flanging operations is usually designated using the maximum HER. This is obtained by dividing the internal diameter of a flange by the diameter of the minimum hole size needed to form the flange (calculated by, $HER = D_f/D_i$: where D_i is the hole diameter and D_f is the diameter of the inner surface of the flange). The HER depends on the mechanical properties and microstructure of the blank material, the punch geometry, and the hole preparation process [4]. Hole-flanging by stamping is characterized by low HERs [5].

Present demands for the use of lightweight materials that have high strength and stiffness in vehicle construction require manufacturing processes that can form materials with low formability [6]. New hole-flanging process variants are needed to increase formability in hole-flanging. Blanks may be formed in several press strokes using progressive die sets rather than a single press stroke to improve formability in hole-flanging operations. Alternatively, Groche and Erhardt [7] proposed laser-assisted heating of the flange edge (blanks of aluminum and magnesium wrought alloys) to improve formability. In the same way, Motaman et al. [8] increased hole-flange ability by conducting laser-assisted heating of dual-phase steel (DP1000) blanks. The increase in formability was attributed to the dynamic strain ageing of the steel. These process variants lead to higher formability. However, they increase equipment costs and process time.

Non-conventional forming processes such as electromagnetic forming (EMF) have been applied to hole-flanging [9]. Sow et al. [10] optimized the shapes of aeronautic components having flanges with elementary geometries (straight, convex, concave, circular, and jogged flanges) formed by EMF. EMF produces flanges with high formability, low spring back, and high surface quality. However, only workpieces made from suitable materials that are electromagnetic can be formed using this method, and the process is still in the development stage. Hence, new process variants are needed to meet high formability requirements at low costs. Cost reduction may be achieved by using dieless forming processes, which eliminate or minimize the use of dies [11]. In addition, Abele et al. [12] proposed using the same equipment to make a variety of products (machine flexibility) to minimize cost.

Hole-flanging by single point incremental forming (SPIF) with multiple forming stages was introduced by Cui and Gao [13] to benefit from the dieless nature and low equipment cost of SPIF processes. In the process, a tool is programmed to follow pre-defined tool paths on a computer numerical control (CNC) machine center and progressively expand holes in clamped sheets to form flanges. Low equipment cost, high formability and process flexibility make hole-flanging by SPIF ideal to produce small batches of flanges [14]. However, poor geometrical accuracy and a long process time have caused a slow take-up of hole-flanging by SPIF in the forming industry as stated by Bambach et al. [15]. Borrego et al. [16] explored single-stage incremental hole-flanging by SPIF to reduce the process time. This strategy leads to a drop in formability compared to multi-stage strategies. Cao et al. [17] developed a 'featured tool' to improve the blank thickness distribution and formability of flanges formed by hole-flanging using single-stage SPIF. The featured tool had limitations in forming flanges with small wall radii. Laugwitz et al. [18] investigated high-speed incremental hole-flanging on a lathe machine to reduce process time. The process set up limits the blank sizes that can be formed and is ideal for research rather than industrial use. However, the setup showed that axisymmetric hole-flanging can be sped up considerably compared to standard hole-flanging by SPIF.

The process variants outlined above to improve formability in hole-flanging have limitations, as demonstrated. A novel hole-flanging process that combines the high formability of incremental forming processes and a short process time (~ 2 s) was presented by Besong et al. [19]. It draws upon paddle forming, in which a paddle-shaped tool rotating at high speed induces heat and shear on a blank to improve formability. A rise in blank temperature due to high-speed punch rotation can improve formability in conventional hole-flanging. Formability increases at high temperatures, as shown by Zhang et al. [20]. The paddle forming process variant requires a paddle tool mounted on a spindle driven at high speeds and may not always be easily integrated into existing production lines. To allow for high formability in existing conventional hole-flanging set-ups and without a loss in productivity, the use of punch rotation with a solid ball-shaped tool is explored. This new variant is called hole-flanging with punch rotation. Along similar lines, Allwood and Shoulder [21] proposed adding shear to sheet metal forming operations when possible to improve formability. The first step towards hole flanging with punch rotation was undertaken by Thiruvarudchelvan [22] as far as the authors are aware.

The setup of hole flanging with punch rotation is shown in Fig. 1. The blank is held using a clamp and die as in conventional hole-flanging, see Fig. 1a. A punch moves to expand the pre-drilled hole while rotating at sufficiently high speeds as shown in Fig. 1b, and c. The forming operation is completed when the punch reaches the flange height in
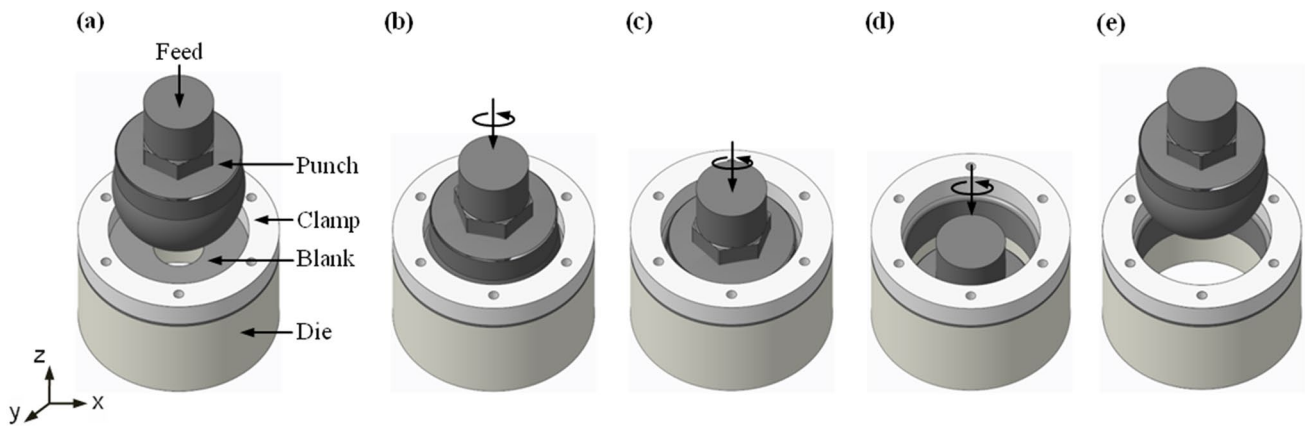
Fig. 1 Hole-flanging by stamping with punch rotation

Fig. 1d. The punch returns to its original position above the assembly as at the end of the process, in Fig. 1e. The forming time depends on the punch feed and the flange length and can be kept in the range of typical flanging operations in the forming industry. The main hypothesis is that this new process will keep the process time in the order of magnitude of typical stamping processes while increasing formability because of a rise in blank temperature and the influence of shear. In contrast to hole flanging by a conventional stamping process, the new process variant generates heat and shear which are coupled with the punch rotation and feed.

Aim of the research

The current investigations on hole-flanging with punch rotation were conducted to achieve the following objectives:

- to increase the formability in hole-flanging by using punch rotation at varying feeds and speeds.
- to control the temperature in the hole flanging tests on a conventional milling machine to form flanges with the maximum formability.
- to determine the maximum HER of the flanges made by conventional stamping and stamping with punch rotation.
- to find the range of punch speeds and axial feeds (process window) required to form flanges of specific HERs. The variation of the blank temperature is used to explain the process window.
- to explain the difference in the maximum HER of hole-flanging process variants by using the influence of the process temperature, shear, and strain rate.

The paper is structured as follows. The material and methods used to describe the forming mechanisms and material forming limits are presented in Section 2. The results and discussions on the FE simulations and experiments of the hole-flanging process variants are shown in Section 3. Section 4 presents the conclusions and outlook.

Materials and methods

Tensile tests

Blanks from the same batch of the aluminum alloy EN AW-6181-T1 with 0.8 mm thickness investigated in [19] were used to conduct the experiments. Aluminum blanks are ideal for warm working. Geiger and Merklein [23] stated that at 250 °C, the elongation of the Aluminium is about 3 times that at room temperature, and the flow stress decreases by 50% compared to room temperature.

Hot tensile tests were carried out on a dilatometer DIL805 machine using test specimens of the blank material having the dimensions shown in Fig. 2. The tensile tests were conducted in the rolling direction of the blank at different temperatures and strain rates to find out the variation of
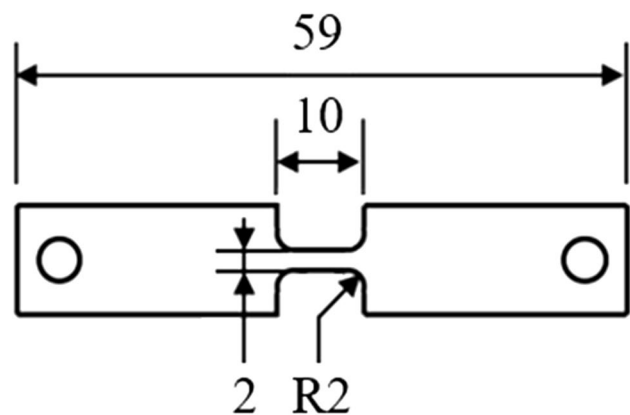

Fig. 2 Dimension of the specimens used to conduct hot tensile tests in the dilatometer

formability. The specimens were heated using induction coils in a vacuum of 10^{-4} bar. Thermocouples were welded in the middle of the test specimens. The temperature was maintained constant in the tests. True stress–strain curves were obtained for test specimens deformed at 25 °C, 300 °C, 350 °C, 400 °C, and 450 °C. To determine the influence of the strain rate, hot tensile tests were performed using strain rates of 1 s^{-1}, 0.1 s^{-1}, and 0.01 s^{-1} at 350 °C.

Finite element model

Virtual forming by FE simulations provides the possibility to determine the feasibility of metalworking processes and reveal the influence of process parameters. The temperatures in numerical simulations can serve as guidelines to achieve process control in the new process variant and maintain the process formability within defined limits. FE simulations were conducted to find out the correlation of punch rotation with the process temperature and forming load. From the FE simulations, the optimal parameters for the experimental design and process control can be determined. The blanks were modeled as deformable shells with 7 fully integrated points in the through-thickness of the sheet. The blanks were assumed to be isotropic and the mechanical properties were assigned using the values in Table 1. Fixed boundary conditions were used to clamp the blanks. The punch and die were considered as rigid bodies in the FE model setup. The conventional hole-flanging simulation was conducted with a punch feed of 1500 mm/min and no punch rotation. Hole flanging with punch rotation was carried out with a punch feed of 1500 mm/min and the punch was rotated at a speed of 6000 rev/min. The simulations were executed on the coupled structural and thermal solvers of LS-DYNA implicit dynamic with double-precision (ls-dyna_smp_d_R11). The thermal and mechanical solvers were assigned variable time steps. The displacement convergence tolerance in the solution control was set to 0.05.

Thermomechanical material model

The flow stress of the material was defined by the Johnson–Cook flow stress model, which depends on the strain, the strain rate and the temperature, see Eq. 1.

$$\tilde{\sigma} = \left(A + B\varepsilon_p^n\right)\left(1 + Cln\frac{\dot{\varepsilon}_p}{\dot{\varepsilon}_0}\right)\left(1 - \left(\frac{T - T_r}{T_m - T_r}\right)^m\right) \quad (1)$$

where $\overline{\sigma}$ is the flow stress, A and B are the strain hardening coefficients, C defines the strain rate strengthening coefficient, ε_p^n is the plastic strain, $\dot{\varepsilon}_p$ is the effective plastic strain rate, $\dot{\varepsilon}_0$ is the reference equivalent strain rate, T is the temperature of the blank, T_r is room temperature, and T_m is the melt temperature. n describes the strain hardening and m is the thermal softening exponent. The values of the Johnson–Cook flow stress model were determined by matching the stress-stress curves of the hot tensile tests. The coefficient of friction between the punch and blanks was determined by parametrization of the hole-flanging FE simulations in Ls Opt software to obtain forces and temperatures with the same magnitudes as in the experiments.

Thermal model

There is an increase in blank temperature due to friction at the contact of the tool and blank [19]. The thermal energy Q generated per unit area at the contact between the sliding surfaces is obtained by:

$$Q = \mu P\left(V_1 - V_2\right) \quad (2)$$

where P is the contact pressure between the surfaces, μ is the coefficient of friction, V_1 is the velocity of the punch and, V_2 is the velocity of the blank. The rate of heat flow through the blank is expressed as:

$$\frac{\Delta Q}{\Delta t} = -kA\frac{\Delta T}{\Delta x} \quad (3)$$

where ΔQ is the net heat transfer, Δt is the time interval required to transfer heat, k is the thermal conductivity, ∇T is the temperature difference between 2 points, A is the surface area and Δx is the distance between 2 points. An additional increase in blank temperature may be caused by the conversion of plastic work from the deformation of the blank into thermal energy, because of the fast-forming rate. Heat loss due to radiation and convection was not included in the FE simulations since the process time is short. The thermal conductivity and the specific heat were assigned as 237 W/m K and 0.92 kJ/kg K for aluminum and 52 W/m K and 0.48 kJ/kg K for steel, respectively.

Table 1   Mechanical properties of EN AW-6181-T1

E(GPa)	A(MPa)	B(MPa)	T_m(°C)	T_r(°C)	C	n	m
70	114.5	347.56	650	25	0.0628	0.23	0.71

Determination of the process mechanics through finite element simulations

The first law of thermodynamics states that the total energy of a system ε can be expressed as the total power entering the system [24].

$$\frac{d\varepsilon}{dt} = Pe + Qe \tag{4}$$

The variation of ε is expressed as Eq. (5).

$$\underbrace{d\varepsilon}_{\substack{variation\ of \\ total\ energy}} = \underbrace{Pedt}_{\substack{mechanical \\ power}} + \underbrace{Qedt}_{\substack{thermal \\ power}} \tag{5}$$

For a volume, the internal energy $\mathcal{U}$ is defined by:

$$\mathcal{U} = \int_V \rho u dV \tag{6}$$

The change in the kinetic energy $d\mathcal{K}$ describes the displacement of the volume.

$$d\mathcal{K} = \frac{d}{dt}\int_{V_t \equiv V} \frac{1}{2}\rho V^2 dV \tag{7}$$

The total energy ε is equal to the sum of changes in the internal and kinetic energies

$$\frac{d\varepsilon}{dt} = \frac{d\mathcal{K}}{dt} + \frac{d\mathcal{U}}{dt} = \frac{d}{dt}\int_{V_t \equiv V} \frac{1}{2}\rho V^2 dV + \int_V \sigma : D dV + \int_V \rho r dV - \int_{\partial V} q : n dS \tag{8}$$

where ρ is the mass density, V is a volume bounded by a surface S, σ is the Cauchy stress tensor, D is the rate of deformation (strain tensor), q represents the heat flux, r is the heat production rate and n is the unit normal. The kinetic energy is not stored as the internal energy of the volume. Hence the total internal energy $d\mathcal{U}$ of the volume is

$$\frac{d\mathcal{U}}{dt} = \frac{d}{dt}\int_{V_t \equiv V} \rho u dV = \int_V \sigma : D dV + \int_V \rho r dV - \int_{\partial V} q : n dS \tag{9}$$

The mechanical contribution of the internal energy of the volume is determined by $\int_V \sigma : D dV$. The variation of the heat energy in the medium with time is given by $\int_V \rho r dV - \int_{\partial V} q : n dS$

For a very small volume, the integral can be dropped (Reynold's Lemma and the divergence theorem). Hence Eq. (9) reduces to

$$\rho u = \sigma : D + (\rho r - qn) \tag{10}$$

From the infinitesimal strain theory, strain $D = \dot{\varepsilon}$ Eq. (11)

$$\underbrace{\rho u}_{\substack{internal \\ energy\ density}} = \underbrace{\sigma : \dot{\varepsilon}}_{\substack{mechanical \\ power}} + \underbrace{(\rho r - qn)}_{\substack{thermal \\ power}} \tag{11}$$

The strain is comprised of a plastic deformation and elastic deformation $\dot{\varepsilon} = \varepsilon^{pl} + \varepsilon^{el}$. FE simulations were conducted to study the forming mechanics of hole-flanging by conventional stamping and stamping with punch rotation. Using a similar procedure as in Maqbool and Bambach [25], the quantitative contributions of membrane stretching, bending, and shear to the deformation mechanisms in the process variants were obtained by splitting the plastic energy density. The plastic energy density is defined by:

$$E_{plastic} = \int_0^t \sigma_{ij} : \varepsilon_{ij}^{pl} dt \tag{12}$$

where σ_{ij} = stresses, ε_{ij}^{pl} = plastic strains, t = process time, and indices $i, j \in \{1, 2, 3\}$ are the principal axes. The plastic energies from the simulations are the sum of the deformation energies due to membrane stretching, bending, and shear:

$$E_{plastic} = E_{stretching} + E_{shear} + E_{bending} \tag{13}$$

The energy densities were calculated using the average of the integration points through the sheet thickness. The shear energy is obtained by substituting the out-of-plane shear stresses (σ_{13}, σ_{23}) and strains ($\varepsilon_{13}^{pl}, \varepsilon_{23}^{pl}$) from the FE simulations into Eq. (12). The plastic energy due to the normal stresses-strains $\left(\sigma_{33} : \varepsilon_{33}^{pl}\right)$ and the out-of-plane shear components are added together because the normal stresses-strains and the out-of-plane shear have the same effect in preventing blank failure and enhancing formability [26]. The membrane stresses obtained from the simulations contain the combined effects of bending and membrane stretching deformation mechanisms.

$$\sigma = \sigma_b + \sigma_s \tag{14}$$

where the membrane stresses, $\sigma = (\sigma_{11}, \sigma_{22}, \sigma_{12})$, the bending stresses $\sigma_b = (\sigma_{b11}, \sigma_{b22}, \sigma_{b12})$, and the membrane stretching stresses $\sigma_s = (\sigma_{s11}, \sigma_{s22}, \sigma_{s12})$. For a perfect plastic bend and using the bending moments obtained from the simulations, the bending stresses are obtained as;

$$M_p = \frac{\sigma_b h^2}{4} \Rightarrow \sigma_b = \frac{4M_p}{h^2} \tag{15}$$

where the bending moments, $M_p = (M_{11}, M_{22}, M_{12})$, and h is the sheet thickness.

The bending stresses from Eq. (15) and the corresponding membrane strains $\left(\varepsilon_{11}^{pl}, \varepsilon_{22}^{pl}, \varepsilon_{12}^{pl}\right)$, from the simulations are substituted into Eq. (12) to obtain the bending energy. The membrane stretching energies are determined by substituting the plastic energy densities from the simulations, the shear energies, and bending energies into Eq. (13). The energy splitting method is validated if the energies from the

deformation modes sum up to the plastic energy density. Thermal energy density is discussed separately with the temperature evolution of the blank.

Forming limit estimation with the M–K model

Forming limit diagrams (FLD) developed by Keeler and Backhofen [27] are commonly used to describe and evaluate the formability of sheet metals under various forming conditions. The FLD of a material is obtained by deforming the blank over the range of strain ratios using in-plane and out-of-plane tests. To estimate the forming limits in the FE simulations, a temperature and strain rate dependent failure criterion based on hot tensile tests is needed. The forming limit of the blank material was estimated using the M–K model that assumes an initial geometric imperfection on the blank surface [28]. The model is based on the presumption that the blank material has a shallow groove (zone B) on a flat surface (zone A) as shown in Fig. 3a. This groove leads to an inhomogeneity factor, f defined by Eq. (16).

$$f_0 = \frac{t_0^B}{t_0^A} \tag{16}$$

$$f = f_0 \cdot exp\left(\varepsilon_{zz}^b - \varepsilon_{zz}^a\right) \tag{17}$$

t_0^B is the blank thickness in the groove and t_0^A is the blank thickness at the surface. f_0 has a major influence on the forming limit strains. The groove can be rotated at any angle, θ between 0 and 180 in the global coordinate during deformation. The strains-stresses tin the global coordinates are converted to the groove coordinates by Eq. (18).

$$\widetilde{\sigma} = \beta_\theta^t \cdot \sigma \cdot \beta_\theta; \widetilde{\varepsilon} = \beta_\theta^t \cdot \varepsilon \cdot \beta_\theta \tag{18}$$

T_θ is a rotation matrix, T_θ^t is the transpose of the matrix.

$$\beta_\theta = \begin{bmatrix} cos\theta & sin\theta & 0 \\ -sin\theta & cos\theta & 0 \\ 0 & 0 & 1 \end{bmatrix} \tag{19}$$

The groove angle is updated using Eq. (20) as deformation progresses.

$$tan(\theta + d\theta) = tan(\theta)\frac{1 + d\varepsilon_{xx}^A}{1 + d\varepsilon_{yy}^A} \tag{20}$$

Assuming surface traction occurs in both zone A and zone B, the stresses perpendicular to both regions are considered equal, Eq. (21).

$$\sigma_{zz}^A = \sigma_{zz}^B; \ \sigma_{z1}^A = \sigma_{z1}^B; \ \sigma_{z2}^A = \sigma_{z2}^B \tag{21}$$

The stresses in region B are obtained using the force equilibrium at the boundary of region A and region B.

$$\begin{cases} \sigma_{22}^B t^B = \sigma_{22}^A t^A \\ \tau_{12}^B t^B = \sigma_{12}^A t^A \end{cases} \Rightarrow \begin{cases} \sigma_{22}^B = \sigma_{22}^A/f \\ \tau_{12}^B = \sigma_{12}^A/f \end{cases} \tag{22}$$

The strain compatibility between the homogeneous and inhomogeneous regions is stated as

$$d\varepsilon_{11}^B = d\varepsilon_{11}^A \tag{23}$$

The increments of the strains ($d\varepsilon$) and stress ($d\sigma$) in the groove and surrounding blank are obtained based on the true stress–strain curves of tensile tests input into the M–K model, obeying an isotropic von Mises plasticity. A set of nonlinear equations are solved to obtain the stresses and strains until the fracture strain. The material in zone B deforms at a faster rate than in zone A until the effective strain at zone B becomes 10 times the effective strain of zone A, which leads to plastic instability and fracture.

The M–K model was used to simulate the hot tensile tests performed in the dilatometer, see Section 2.1. The true stress–strain curves from the hot tensile tests were used to
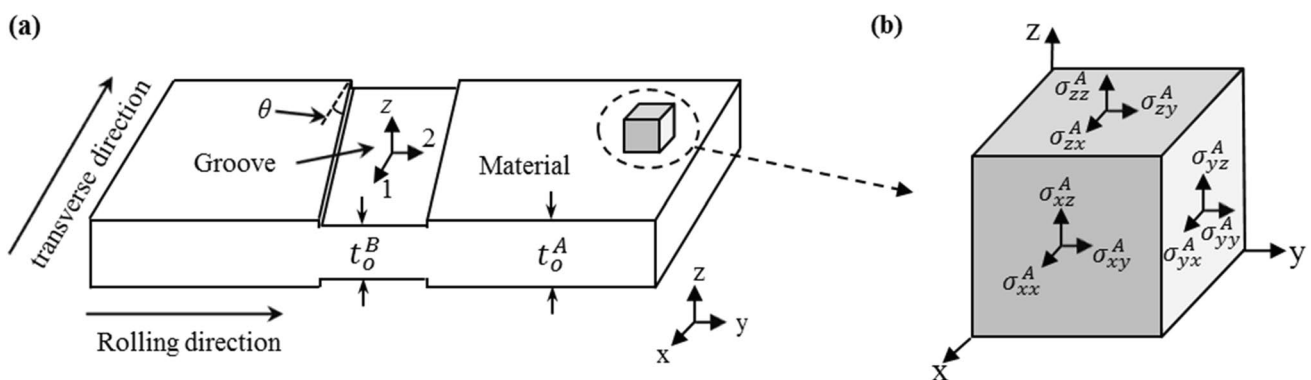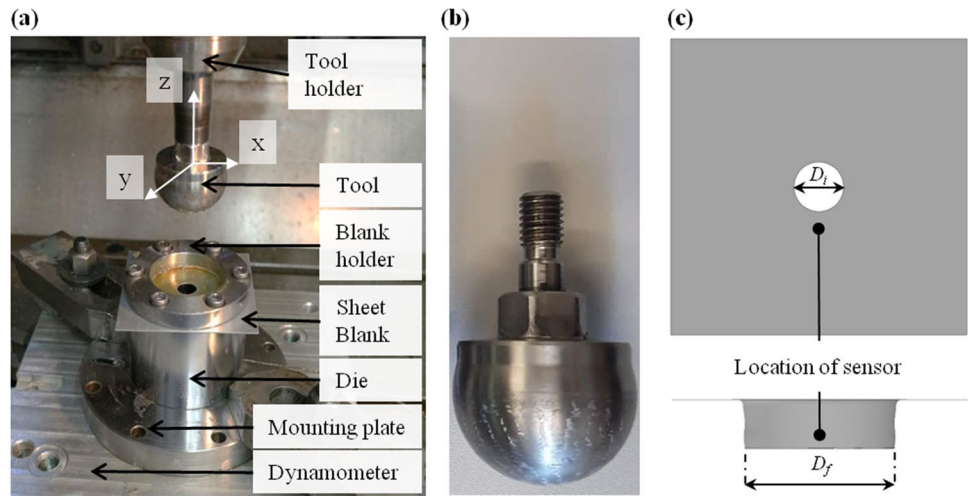

Fig. 3 **a** Schematic of a defect used in the M–K model. **b**) Stress state of an element in zone A of the sheet

Fig. 4 a Experimental setup of hole-flanging with punch rotation. (**b**) Punch used in experiments. (**c**) Location of the thermocouple on the blank before and after hole-flanging

define the mechanical properties of an S4R shell element. The inhomogeneity factor (f_0) was varied so that maximum true strains (elongation at break) from the FE simulations of the M–K model match the fracture strains in the hot tensile test experiments. 100 imperfections with 0° initial angles were used in all the analyses. All the critical values of the deformation severity were set equal to zero [29]. The M–K model provides a rough estimate of forming limits of the material at different temperatures and strain rates. The M–K model is not included in the simulations of process variants.

Process forming limits in terms of the stress triaxiality and equivalent stress

The M–K formability model is implemented only for plane stress ($\sigma_{13}, \sigma_{23}, \sigma_{33} = 0$) element types in ABAQUS software and it can estimate the forming limits of forming operations that occur mainly by in-plane stretching. However, hole-flanging by stamping with punch rotation is characterized by out-of-plane deformation that includes the effects of out-of-plane stresses-strains. In addition, the strain paths in the hole-flanging process variants may differ from those in the tensile tests. The forming limits of the process variants were also expressed as a variation of the stress triaxiality and the equivalent plastic strains. The stress triaxiality η is the ratio of the hydrostatic stress to the equivalent stress, calculated by.

$$\eta = \frac{\sigma_h}{\tilde{\sigma}} \tag{24}$$

where the hydrostatic stress is $\sigma_h = \frac{\sigma_{11}+\sigma_{22}+\sigma_{33}}{3}$ and the equivalent stress is.

The equivalent plastic strain, $d\bar{\varepsilon}$ is defined by

$$d\bar{\varepsilon} = \sqrt{\frac{2}{3}\left[\left(d\bar{\varepsilon_1}\right)^2 + \left(d\bar{\varepsilon_2}\right)^2 + \left(d\bar{\varepsilon_3}\right)^2\right]} \tag{25}$$

where $d\bar{\varepsilon_1}$, $d\bar{\varepsilon_2}$, and, $d\bar{\varepsilon_3}$ are the plastic strain in the principal directions. The forming limit is attained when the ductile damage criterion D, is reached.

$$D = \int_0^{\varepsilon f} \frac{\sigma_h}{\tilde{\sigma}} d\bar{\varepsilon} \tag{26}$$

where ε_f is the equivalent plastic strain at fracture. The forming limits were determined to obtain a simple approach to maximize the process formability.

Setup of hole-flanging experiments

The setup of stamping with punch rotation is shown in Fig. 1. The blanks were clamped using the same clamp and die in the 2 hole-flanging process variants, see Fig. 4a. The die and blank holder had 42 mm inner diameters. Holes with initial diameters (D_i) were cut in the blanks using a milling cutter. The minimum hole diameter needed to form flanges for each process variant was found. Stamping with punch rotation was conducted on blanks with hole diameters of 12 mm and 10 mm corresponding to HERs of 3.3 and 4, respectively. A punch with a diameter of 40 mm was used to form the flanges, see Fig. 4b. The same punch was used in conventional hole-flanging and stamping with punch rotation. The punch was fixed in the conventional hole-flanging

$$\tilde{\sigma} = \sqrt{\frac{1}{2}\left[\left(\sigma_{11} - \sigma_{22}\right)^2 + \left(\sigma_{22} - \sigma_{33}\right)^2 + \left(\sigma_{33} - \sigma_{11}\right)^2\right] + 3\left(\tau_{12}^2 + \tau_{23}^2 + \tau_{31}^2\right)}$$

Fig. 5 Tensile test results. (**a**) Effect of temperature. (**b**) Effect of strain rate
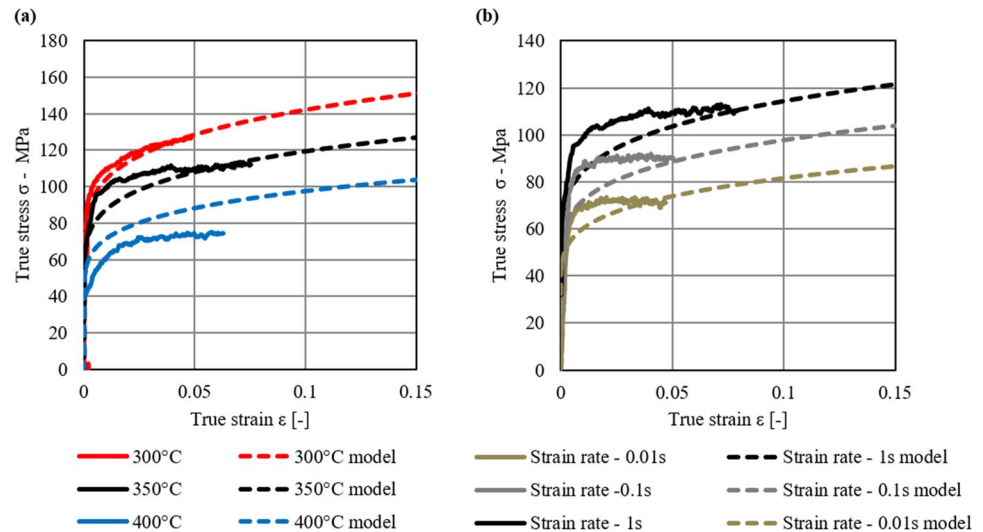
experiments while it was rotated in stamping with punch rotation. The flanges were formed between punch feeds of 250 mm/min and 3000 mm/min. The punch speed varied from 1000 rev/min to 6000 rev/min. The blank material adhered to the punch surface, and the punch was cleaned after every few tests using sandpaper. Raziol CLF 100 cold forming oil was used as a lubricant in the tests.

The temperatures of the blanks were measured close to the hole by using thermocouples glued on the outer surface of the blank during the forming processes, see Fig. 4c. A dynamometer was used to measure the forces in the forming processes. The assembly of the dynamometer and die set were clamped on the machine bed as shown in Fig. 4a. A data acquisition system was used to record the blank temperature and forming forces. A vertical milling machine center Arrow 1000 was used to conduct the experiments.

Grids with a point distance of 2 mm and a point diameter of 1 mm were etched on the outer surfaces of all the blanks. GOM argus® photogrammetry system was used to measure and analyze the deformation of the formed flanges. The principal strains are obtained by comparing the grid point distances on the outer side of the formed flange to the non-deformed blank before forming. The principal strain measurements in this study are 'logarithmic principal surface stretches' because punch rotation causes significant shear [30].

Results and discussion

Finite element Simulation

The Johnson–Cook material law that matched the hot tensile tests is shown for the strain rates and some temperatures in Fig. 5. The parameters of the material law are presented in
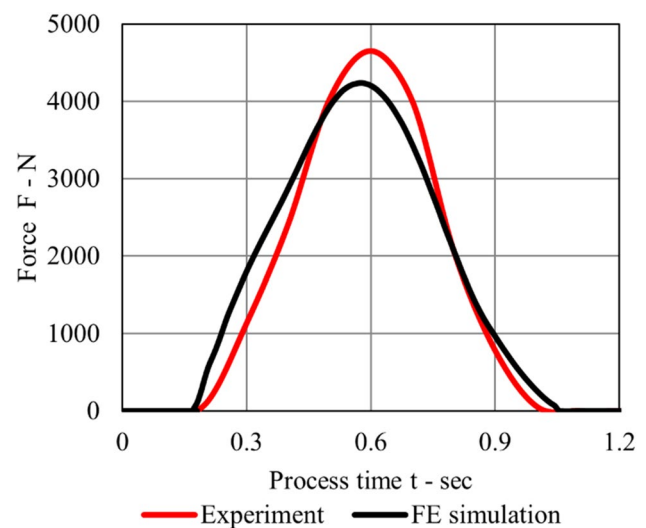

Fig. 6 Forces in hole flanging of a flange with an initial hole diameter of 27 mm (experiment and FE simulation)

Table 1. The coefficient of friction between the punch and blanks was determined to be 0.12.

Force and temperature variation

The forces from the experiments and FE simulations of conventional hole flanging are presented in Fig. 6. The initial hole size was 25 mm, which represents the maximum HER, based on the results in [19]. The blank temperature remained at approximately 25 °C in conventional hole flanging.

The initial hole size was reduced to 10 mm diameter in stamping with punch rotation based on the high formability reported in [19]. High temperatures were obtained in the hole-flanging with punch rotation, compared to conventional

Fig. 7 a Temperature distribution of flange obtained from FE simulations of hole-flanging with punch rotation. (**b**) The temperature of element A in hole-flanging with punch rotation and conventional hole-flanging. (**c**) The z-forces acting on the punch in hole-flanging with punch rotation and conventional hole-flanging
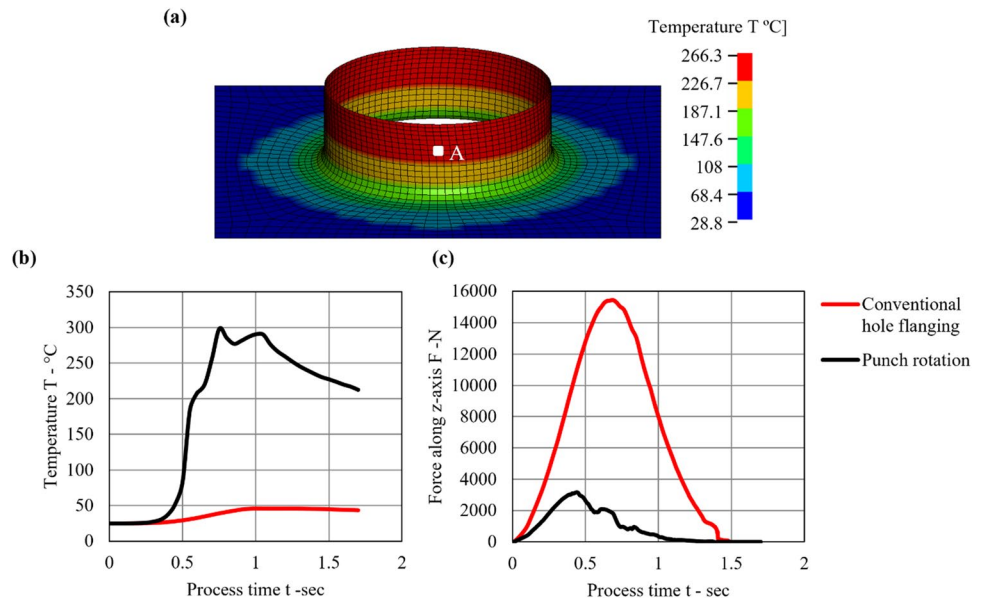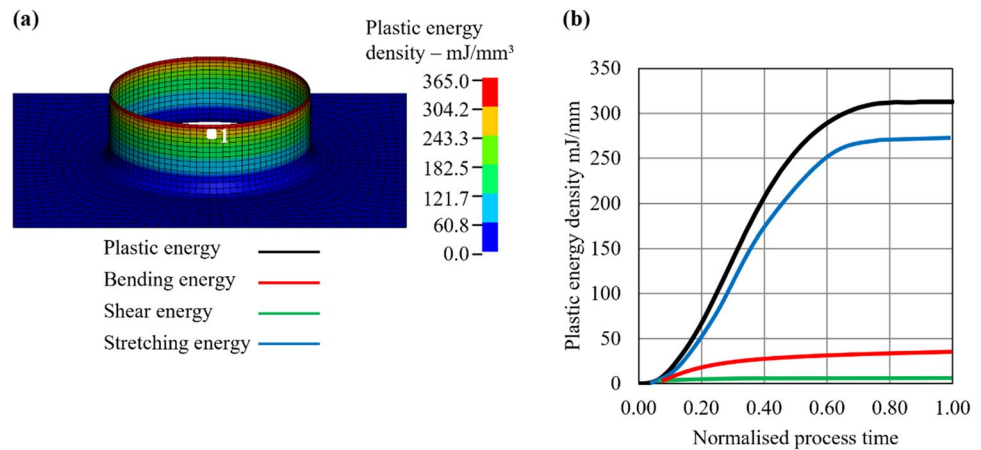

Fig. 8 a Element considered for energy density analysis in conventional hole-flanging. (**b**) The energy density split of element 1

hole-flanging, as shown in Fig. 7b. The high temperature in hole-flanging with punch rotation is due to friction at the contact of the blank and punch, and a high rate of material deformation. The blank temperature increases with an increase in the flange length because there are a higher number of contacts between the rotating punch and blank as the flange length increases. The temperature distribution of a flange formed at a spindle speed of 6000 rev/min and feed of 1500 mm/min at the process end is shown in Fig. 7a. The temperature of element A, which corresponds to the position of the thermocouple in the experiments, is presented in Fig. 4c. A maximum blank temperature of 300 °C was achieved at about 0.8 s when the rotating punch and element are in contact, see Fig. 7b.

The forces acting on the punch in the z-direction (direction of tool feed) are presented in Fig. 7c. The forces along the z-axis were higher in conventional stamping than in stamping with punch rotation. This is because thermal softening reduces the stiffness of the material in stamping with punch rotation. The FE simulations demonstrate that punch rotation reduces the forming forces and increases the blank temperature. The effect of the drop in the process forces caused by inhomogeneity of the MK model is not included in the process forces estimated by the FE simulations.

Energy split from FE simulations

To determinate the process mechanics, the plastic energy densities of elements in FE simulations are split using the procedure presented in Section 2.3. An element close to the flange edge (element 1) was chosen for the energy split analyses because fracture usually occurs close to the flange edge in conventional hole-flanging. The deformation mechanism at this point can be used to understand the difference

Fig. 9 **a** Elements along the flange length chosen for the plastic energy density split in hole-flanging with punch rotation. (**b**) Percentage comparison of energy density splits of the 2 process variants for element 1. (**c**) Contribution of deformation modes to the plastic energy density of element 1 in hole-flanging with punch rotation. (**d**) Energy density variation along the flange length in hole-flanging with punch rotation
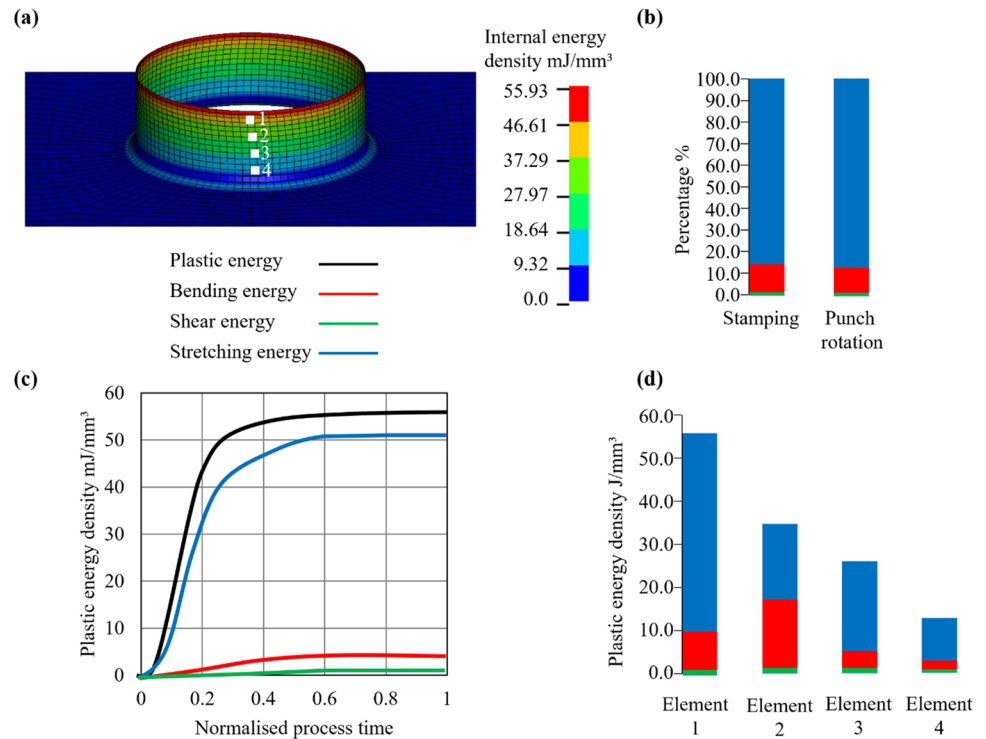
in the formability of the two process variants, see Fig. 8a. The contributions of the deformation modes as a portion of the plastic energy density of element 1 are presented in Fig. 8b. The results indicate that deformation in conventional hole-flanging is achieved primarily by membrane stretching. Bending accounts for about 10% of the plastic energy and the influence of out of plane shear energy is negligible.

To study the forming mechanisms of the flange formed by hole-flanging with punch rotation, the plastic energy densities of 4 elements along the flange length were analyzed in Fig. 9a. Element 1 is next to the flange edge, and element 4 is about 1/4 the flange length from the clamped end. The percentage contribution of the deformation mechanisms determined by the plastic energy densities of element 1 in conventional hole-flanging and hole-flanging with punch rotation are compared in Fig. 9b. The comparison reveals that the forming mechanism is similar in both processes. The plastic energy density is significantly higher in conventional hole-flanging compared to hole-flanging with punch rotation, see Fig. 8b and Fig. 9c. The plastic energy density reduces as the punch is rotated because thermal softening decreases the amount of force (stresses) required to form the blank. This explains the large difference in the magnitude of the maximum plastic energy density obtained from the simulations of conventional hole flanging (365 mJ/mm³) and hole flanging with punch rotation (55.93 mJ/mm³) as shown in Fig. 8a and Fig. 9a. Similarly, the plastic energy density of element 1 reveals a higher plastic energy density in conventional hole flanging. The mechanical power (plastic energy

density) should reduce with an increase in thermal power to obtain a balance of the total internal energy density based on the principle of energy conservation, see Eq. 11. A high plastic energy density indicates that more force is required to achieve the same plastic deformation.

The energy split of element 1 in Fig. 9c reveals that the deformation in hole-flanging with punch rotation occurs mainly by membrane stretching. The bending has a significant contribution to the deformation mode and makes up about 10% of the deformation energy. The out of plane shear energy is negligible. For element 2, deformation occurs mostly by bending rather than membrane stretching, as is expected in hole-flanging operations, as shown in Fig. 9d. This is probably because, at high temperatures (Fig. 7a), the elements in this region require low membrane stretching forces which causes the bending energy to be high as a proportion of the total plastic energy density. However, at the flange edge in element 1, the stretching energy increases to achieve the flange geometry. Negligible shear was present at element 2. The deformation of elements 3 and 4 occurs mainly by membrane stretching. The bending energy was about 11% and 12% respectively, for both elements. Similarly, negligible out of plane shear was detected. The contributions of the forming mechanisms to the deformation of elements 3 and 4 are similar to element 1. The plastic energy density decreases from element 1 to 4 since there is a decrease in blank deformation from element 1 to 4 as the flange length reduces, see Fig. 9d.

Fig. 10 **a** The variation of the true stress–strain curves at different temperatures. (**b**) Estimated forming limits at different temperatures
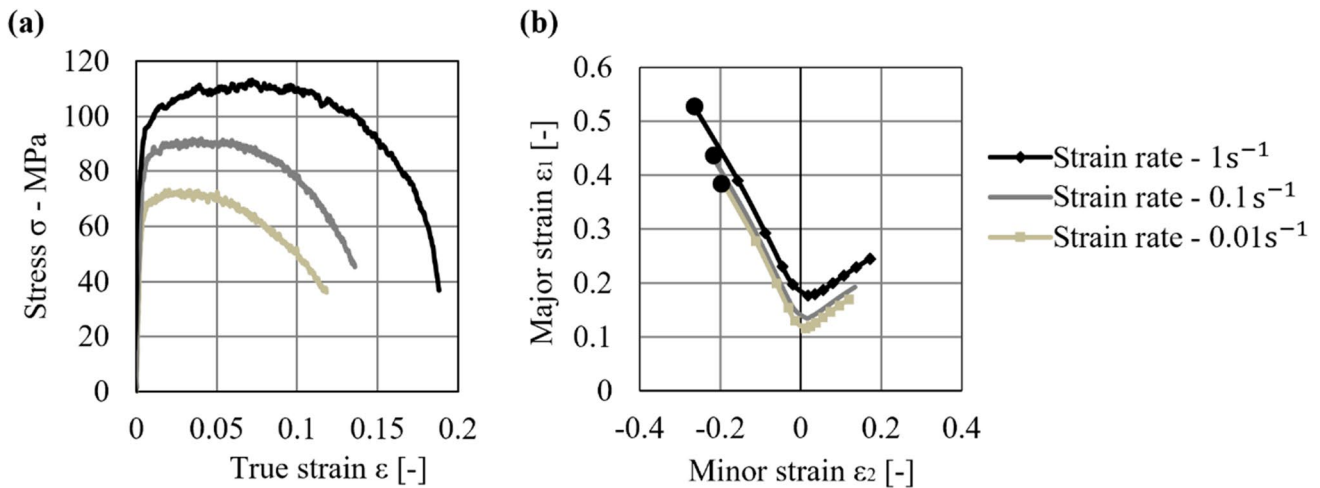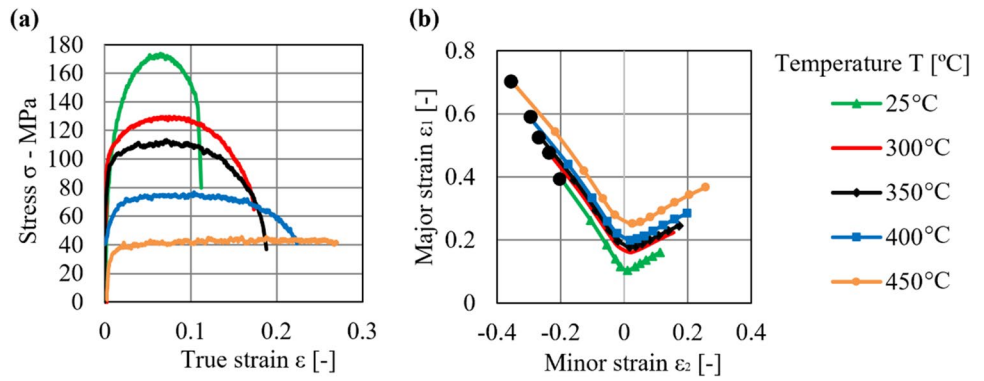

Fig. 11 **a** The variation of the true stress–strain curves at different strain rates. (**b**) Estimated forming limits at different strain rates

Results of the hot tensile tests and forming limit curves obtained by the M–K model

The true stress–strain curves of specimens deformed at 25 °C, 300 °C, 350 °C, 400 °C and 450 °C at a strain rate of 1 s^{-1} were used to study the effect of the temperature on the tensile properties and formability of the blank material. The results show an increase in the maximum true strain (elongation at break) with an increase in blank temperature, see Fig. 10a. There was a drop in the maximum force (stress) required to form the blank at high temperatures.

The M–K model is used to calibrate the failure strains in the FE simulations to the elongation at break of the tensile tests at the different temperatures and strain rates. The elongation at break of the tensile tests in Fig. 10a and Fig. 11a correspond to the black dots along the forming limit curves in Fig. 10b and Fig. 11b. The rest of the points on the forming limit curves are obtained by extrapolating the failure strains using different deformation paths. The FE analyses of the stress–strain curves at different temperatures show that the forming limit curve

(FLC) moves upwards with an increase in temperature. This indicates a rise in formability with temperature since higher blank deformation can be achieved without failure. The reduction in the maximum stress as temperature increases is in line with the first law of thermodynamics, Eq. 11. High blank temperatures in stamping with punch rotation cause a drop in the forming forces due to a decrease in the stiffness of the blank material as observed in Sect. 3.1.1. This is accompanied by an increase in the elongation at break.

Tensile tests conducted at different strain rates reveal a decrease in the maximum stress and strain with a reduction in the strain rate, see Fig. 11a. This is similar to the results of hot tensile tests carried out on AA6061 aluminum alloy at 500 °C [31]. The increased formability at high strain rates at 350 °C is explained by the effect of high-strain-rate superplasticity at high strain rates and temperatures. Figure 11b indicates that there is a movement of the FLC downwards as the strain rate reduces, which shows a drop in formability. The forming limit curves in Fig. 10b and Fig. 11b demonstrate that the formability of the material

Table 2 Groove sizes used in the MK model

Temperature °C	Groove size	Strain rate at 350 °C	Groove size
25	0.98	1	0.87
300	0.9	0.1	0.885
350	0.87	0.01	0.87
400	0.927		
450	0.95		

can be increased by forming the flanges as fast as possible at high temperatures.

The groove sizes used to define the forming limits at different temperatures and strain rates are presented in Table 2.

The FLCs at 25 °C and 450 °C were expressed in terms of the stress triaxiality and equivalent plastic strain obtained from the simulations with the M–K model, see Fig. 12. The formability based on stress triaxiality and equivalent plastic strain is more effective at estimating the forming limits when loading is non-proportional and cyclic strain paths occur [32]. The stress triaxiality ranges from 0,33 (uniaxial tension) to 0,66 (biaxial tension) which is typical of sheet forming operations. The characteristic U-shape of the equivalent

plastic strains in this range of stress triaxiality was observed, see Fig. 12b.

Formability estimation of the hole-flanging process variants

In this section, the forming limits of the hole-flanging process variants were determined using the temperature and strain-rate dependent forming limits based on the M–K model. Conventional hole-flanging occurs at approximately 25 °C and the process limits are described using the forming limit at 25 °C. The equivalent plastic strain of the flange with the maximum HER formed by conventional hole-flanging is shown in Fig. 13a. The evolutions of the stress triaxiality and the equivalent plastic strain of the inner and outer sides of an element at the flange edge are presented in Fig. 13b. The strains from FE simulations in Fig. 13b is close to the forming limit, which implies that the process border for the conventional flanging is reached. The flange had an initial diameter of 27 mm, which corresponds to an HER of 1.48.

Maximum equivalent plastic strains of 0.35 and 0.4 were obtained on the inner and outer surfaces of the element. The higher equivalent plastic strain of the outer surface than on the inner surface indicates an increased tendency for crack

Fig. 12 **a** The FLC at 25 °C and 450 °C. (**b**) The forming limits in terms of the equivalent plastic strain and triaxiality
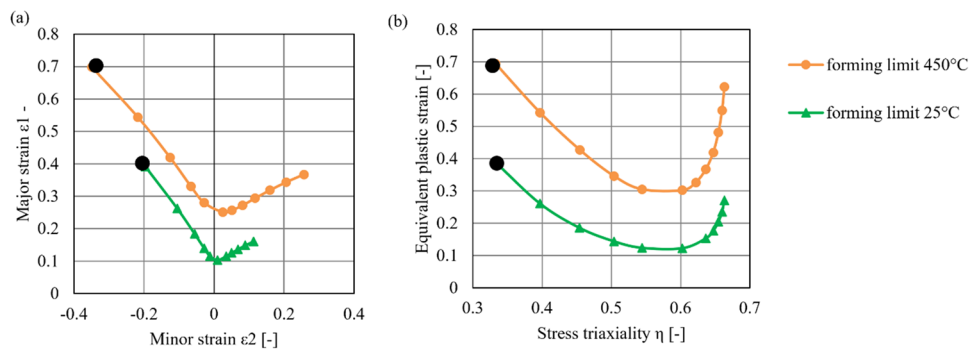

Fig. 13 **a** Flange formed by conventional hole-flanging. **b**) Evolution of stress triaxiality and equivalent plastic strain

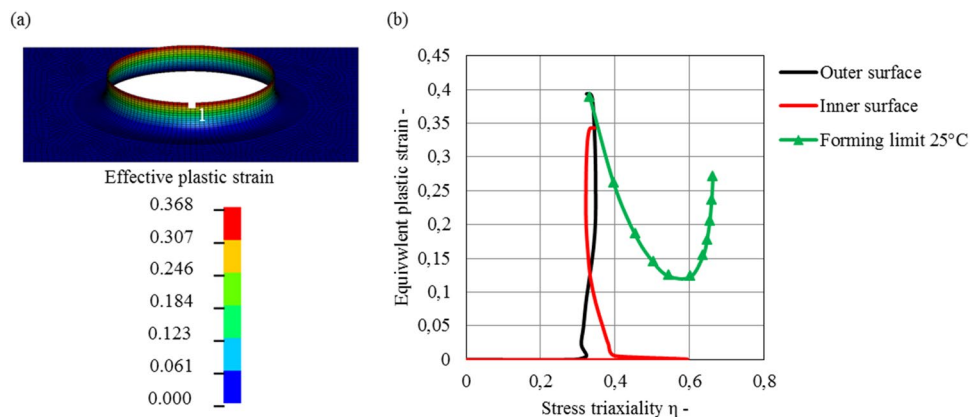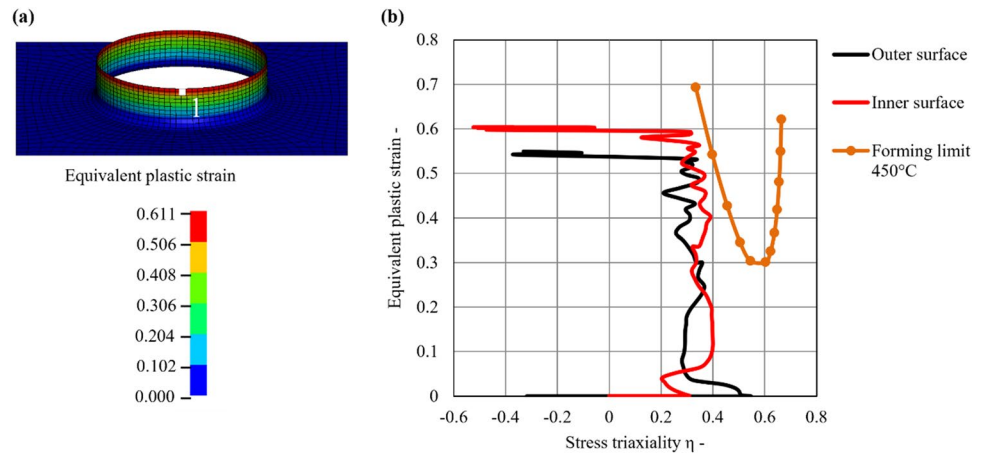**Fig. 14** **a** Flange formed by hole-flanging with punch rotation. **b**) Evolution of stress triaxiality and equivalent plastic strain

development on the outer surface [32]. The stress triaxialities of the inner and outer surfaces of the element were approximately 0.33 during the process. This magnitude of stress triaxiality corresponds to a uniaxial tensile stress state, which is similar to the results obtained by Chung et al. [33] in conventional hole flanging. The stress triaxialities agree with previous observations that deformation occurs in a uniaxial tensile stress state at the flange edge in conventional hole-flanging [1].

Hole-flanging with punch rotation was conducted on a blank with a hole diameter of 21 mm (HER = 1.9). The forming limit of this flange matches the forming limit of the blank at 450 °C. There was a high variation of the stress triaxiality towards the end of the hole-flanging process probably due to high-speed punch rotation and spring back of the blank, as shown in Fig. 14b.

Based on the results of the FE simulations, stamping with punch rotation should have higher formability compared to conventional hole-flanging. Increased formability was observed at high temperatures and strain rates.

Results of hole-flanging with punch rotation

Experiments were conducted to determine the process window and to obtain information about optimal process control. The force and temperature variations with changes in the process parameters are examined. Optical strain measurements were conducted to determine the surface stretch of the formed flanges.

Variation of temperature in hole-flanging with punch rotation

Same as in the FE simulations, the blank temperature increased because of heat generated at the punch-blank contact due to friction caused by the relative motion of the

punch and blank. The temperature variation of flanges with an HER of 4 formed at different punch speeds and feeds are shown in Fig. 15. The rotational speed of the punch was maintained at 6000 rev/min. The maximum blank temperatures were 390ºC for a 500 mm/min punch feed, 275ºC for a 1500 mm/min punch feed, and 170ºC for a 3000 mm/min punch feed, as presented in Fig. 15a. The maximum temperature of the blank reduced as the punch feed increased at a constant punch rotational speed (6000 rev/min). The high blank temperature at 500 mm/min is because the punch makes contact with the blanks for a high number of rotations at low feed rates. The number of contacts between the punch and blanks reduces with an increase in the punch feed that causes less rise in blank temperature. Similarly, there was a reduction in the blank temperature as the punch rotational speed reduced from 6000 rev/min to 5000 rev/min at a constant punch feed of 1500 rev/min as shown in Fig. 15b. This is due to the lower number of contacts between the punch and the blank as the speed of rotation of the punch reduces. The variation of blank temperature with the change in punch feed and speed follow the same trend as reported for the paddle feed and speed in hole-flanging by paddle forming [19].

Change in the forming forces

Negligible forces act in the plane of the sheet (x and y-axis) in hole-flanging by stamping with punch rotation since axisymmetric punch rotation is self-stabilizing in the x and y-axis. The same trend was observed in the variation of the x and y-forces in paddle forming [19]. There is an increase of the forces in the z-direction as the punch feed increases at constant paddle speed, see Fig. 16a. This is because more blank material is deformed per unit time as the punch feed increases. In addition, the heat generated by friction leads to thermal softening of the blank, which reduces the forming forces required to deform the blank at low feeds. The forces in the z-direction increase with a decrease in punch
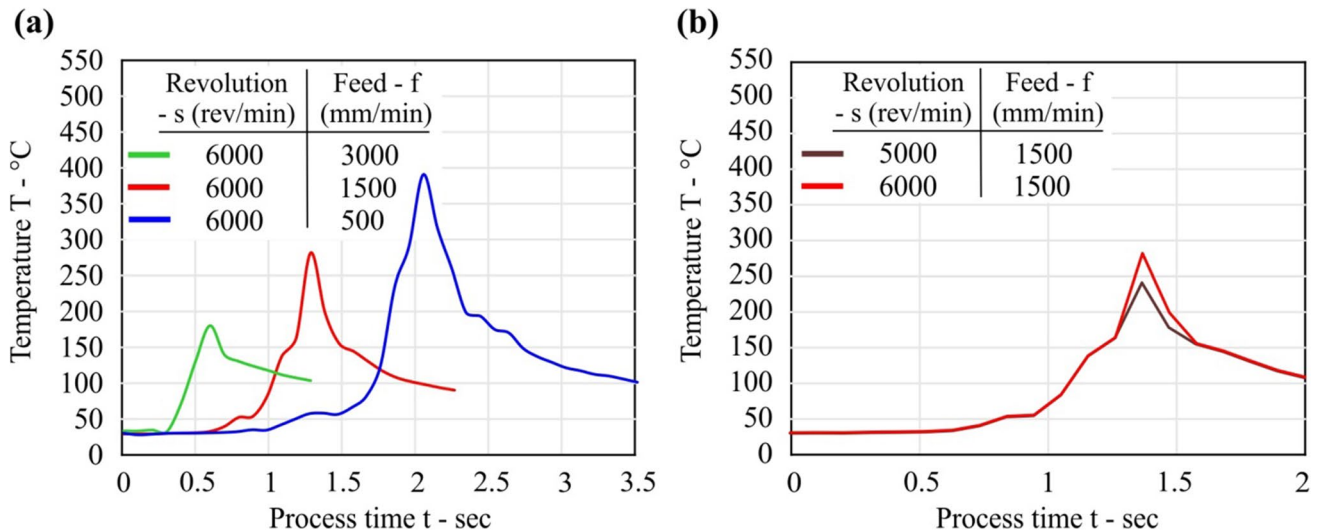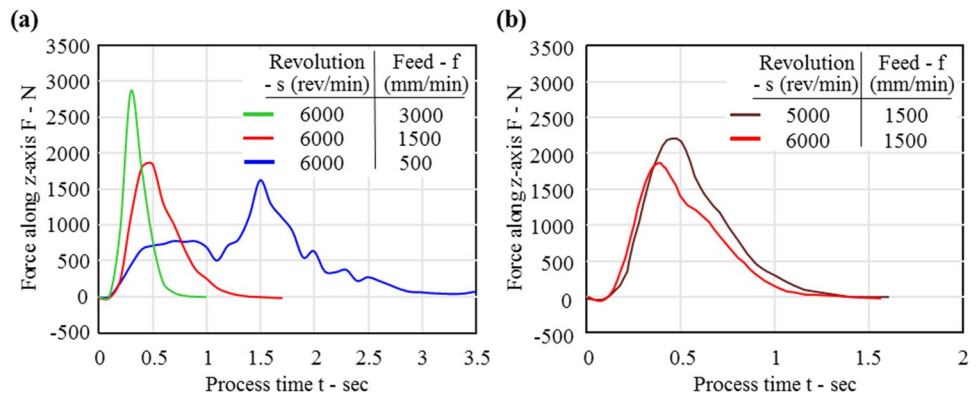
(a)

(b)

Fig. 15 **a** Blank temperature for different punch feeds. (**b**) Blank temperature for different punch speeds

Fig. 16 **a** Change in z-forces with punch feed. (**b**) Change of z-forces with punch speed

(a)

(b)

rotation speed at the same feed rate, as shown in Fig. 16b. This is because low punch speeds cause a drop in blank temperature, which leads to higher forces required to form the blanks.

Experimental strain measurement

Optical strain measurements of the outer surface of the flanges formed by stamping with punch rotation were used to study the deformation of the flanges. A flange with an HER of 3.3 formed by stamping with punch rotation at 6000 rev/min speed and 1500 mm/min feed is shown in Fig. 17a. The major and minor strains of the flange are shown in Fig. 17b and Fig. 17c. The strain distribution on the forming limit diagram of the flange in Fig. 17d is displayed using the legend of the major strain in Fig. 17b. The deformation of the flange is described using a line section, as indicated in Fig. 17c and Fig. 17d. Point A represents the clamped

section of the blank, see Fig. 17c. The blank is not deformed and the principal strains have a magnitude of zero. Point B is the flange bend that corresponds to the principal strains in the wrinkling zone in Fig. 17d. Point C in Fig. 17d is a point located at one-third of the length of the flange with principal strains approaching plane strain deformation ($\varepsilon_2 = 0$). Point D is about two-thirds of the flange length, and the principal strains are close to a plane strain state. The principal strains are approaching uniaxial tension at the flange edge (point E, $\varepsilon_1 = -2\varepsilon_2$), as shown in Fig. 17d. The principal strain measurement of the flange formed by stamping with punch rotation in Fig. 17d reveals a 2-shape curve. Similar 2-shape principal strains were reported by Borrego et al. [34] in axisymmetric conventional hole-flanging of annealed AA7075-O blanks of 1.6 mm thickness. The principal strains of the flanges formed by both processes are primarily in the left quadrant of the FLD. This indicates a similarity of the forming mechanisms in both processes. However, the optical strain measurements of the flanges produced by stamping
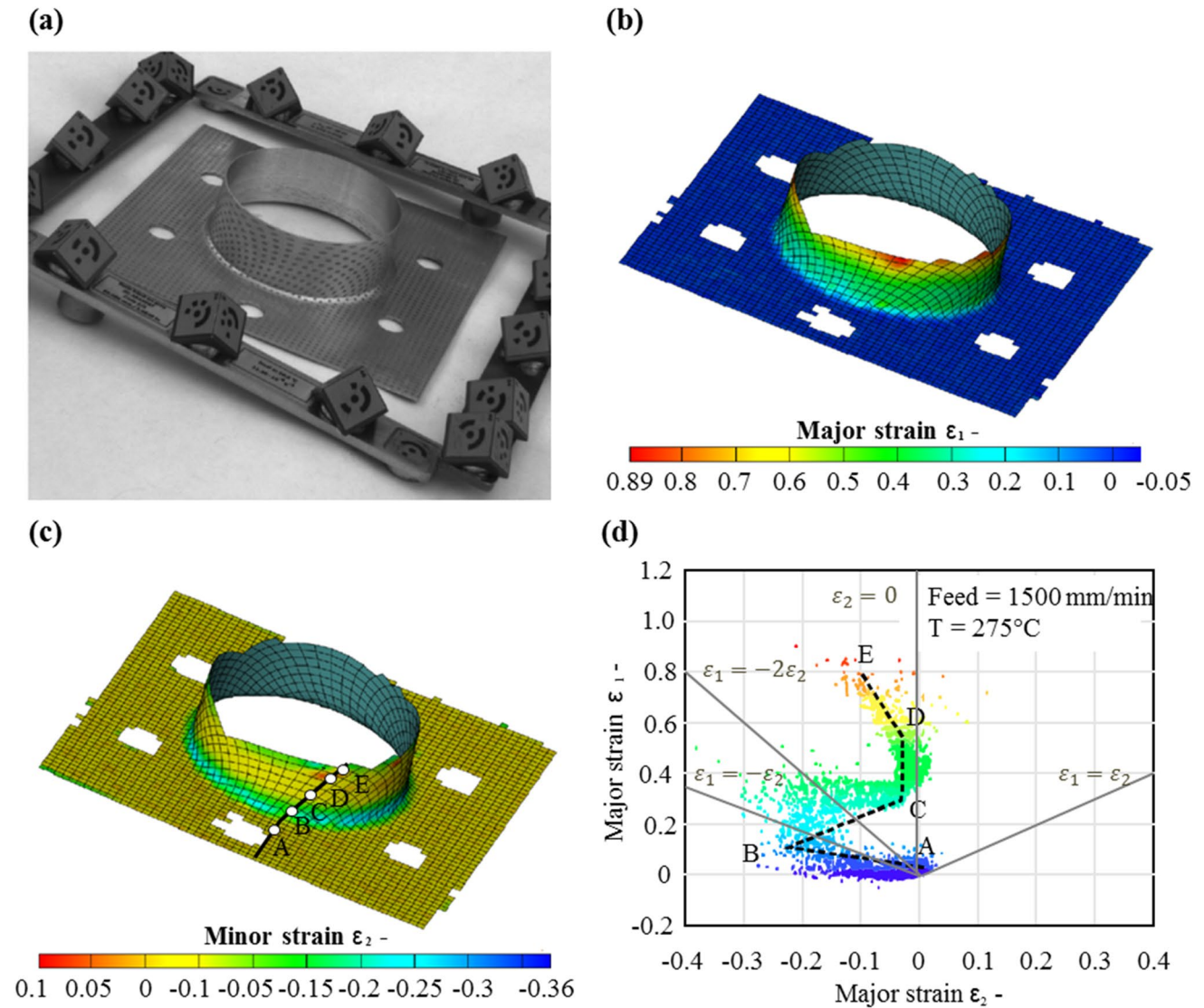
(a)

(b)

Major strain ε_1 -

0.89 0.8 0.7 0.6 0.5 0.4 0.3 0.2 0.1 0 -0.05

(c)

(d)

Minor strain ε_2 -

0.1 0.05 0 -0.1 -0.05 -0.15 -0.2 -0.25 -0.3 -0.36

Fig. 17 a Flange formed by hole-flanging with punch rotation. **b**) Major strain. **c**) Minor strain. **d**) Forming limit diagram

with punch rotation represent logarithmic principal surface stretches, caused by the effects of shear and nonlinear strain paths during the forming process [30].

Process window

In this section, the robustness of the new process is shown using the process window in Fig. 18. The red dots show flanges with cracks, while the green circles represent flanges with no edge cracks. The lines indicate the limits of process parameters needed to form flanges with no cracks.

Figure 18a shows the punch feeds and speeds required to form the flanges with an HER of 4. Flanges were formed at punch speeds between 5000 rev/min and 6000 rev/min. The flanges formed at a punch feed of 500 mm/min and a speed

of 6000 rev/min had cracks. The cracks may be due to a high abrasion of the blank surface by the tool at high punch speeds and low feeds. The results of the flanges having a 3.3 HER indicate that flanges can be formed using a wide range of punch feeds and speeds, Fig. 18b. The process is highly robust, and nearly all the combinations of punch feed and speed can be used to form flanges.

The flange with an HER of 4 had a maximum temperature of 390 °C close to the flange edge, see Fig. 7a. The temperature is probably higher at the flange edge, which may lead to an increase in formability. High strain rates improve formability at high temperatures (350 °C) as demonstrated in the forming limit diagram in Fig. 11b. However, forming at high feed decreases the blank temperature that may cause a drop in formability and crack development. This is observed in

Fig. 18 **a** Process borders of flanges with an HER of 4. **b**) Process borders of flanges with an HER of 3.3
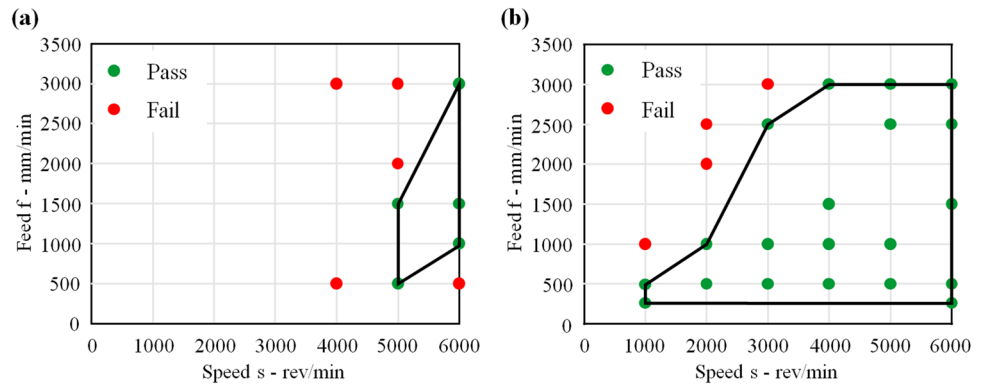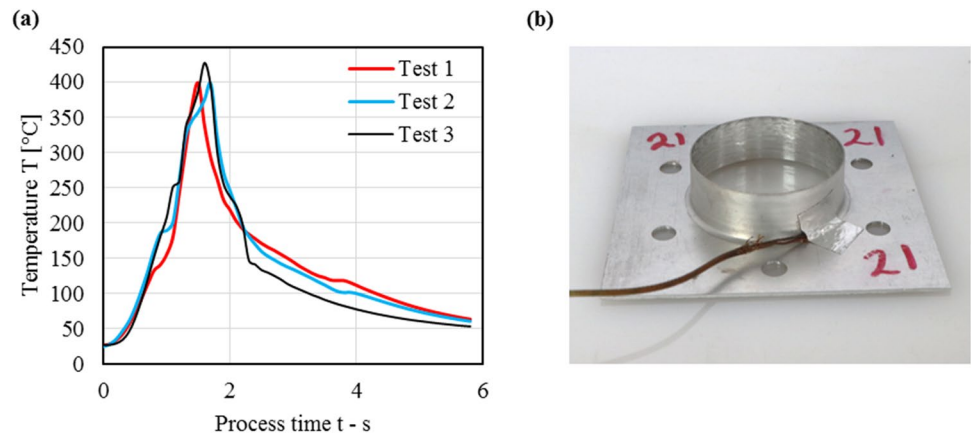

Fig. 19 **a** Blank temperatures for the flanges with an initial hole diameter of 14 mm formed at the same punch speed and feed. (**b**) Position of thermocouple

the flanges with an HER of 3.3 formed at speeds of 1000 rev/min, 2000 rev/min, and 3000 rev/min, see Fig. 18b.

The large diameter of the punch has a reduced ability to locally stretch the blank and cause biaxial stretching [35]. On the other hand, the sharp edges of the paddle stretch the blanks to varying degrees at different paddle speeds and feeds, which causes biaxial tension and a change in the principal strains as reported in [19]. As a result, stamping with punch rotation is more robust compared to paddle forming, which is indicated by the broader range of tool speeds and feeds that can form flanges with an HER of 3.3 in stamping with punch rotation. In addition, Allwood [30] suggested that a smooth contact between the punch and blank may cause surface texturing of the blank that prevents removal of material from the blank surface, compared to the line contact between the blank and paddle in paddle forming that promotes the removal of the blank material. These account for the higher formability (HER = 4) obtained in stamping with punch rotation compared to paddle forming (HER = 3.3) in [19].

Reliability of temperature measurement

To determine the reproducibility of the experimental results in production environments, the temperatures of flanges formed at a punch speed of 6000rev/min and feed of 500 mm/min with 14 mm

initial hole diameters were measured. To ensure accurate blank temperature measurement, a low punch feed rate was used in the experiments to prevent the thermocouple from being detached from the blanks during forming. The maximum flange temperature had a mean value of 411 °C±11. The temperature variation in the 3 test repetitions is approximately the same and demonstrates that the process temperature is stable, see Fig. 19a. The reliability of the results indicates that the process temperature can be pre-defined based on the desired formability and closed-loop process control used to form flanges with high HERs.

The temperatures are higher in these tests compared to the results in Sect. 3.4.1 because the thermocouple elements were welded to the blank instead of glued. The better contact between the blank and the welded thermal element caused higher temperature measurement. The thermocouples were welded very close to the clamped edge of the flanges (Fig. 19b) because welding the blanks at the same position in Fig. 4c may cause an alteration of the microstructure of the blank and early failure during forming.

Flange lengths

The flange lengths changed with variation in punch feed and speed for flanges having the same HER. The flange lengths were between 15.20 mm and 16.90 mm for flanges
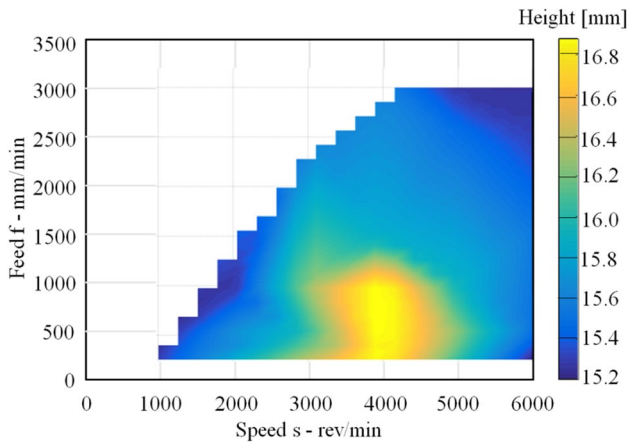
Fig. 20 A representation showing the length of flanges with an HER of 3.3

an increase in flange length compared to the concave tools as revealed from FE simulations [35]. This may explain the reduction in flange length as the punch feed increases.

Conventional hole-flanging

The conventional hole-flanging tests were carried out at 500 mm/min punch speed. The initial hole diameter was varied until the minimum hole size needed to form flanges with no edge cracks was determined. The minimum hole size required to form flanges was found to be 27 mm, which corresponds to an HER of 1.48. This agrees with the forming limits of the process estimated by the equivalent plastic strain and stress triaxiality of the material at 25 °C, see Fig. 13b. Table 3 presents the test results. Flanges with cracks are shown by the crosses (x), while the flanges with-

Table 3 Results of conventional hole-flanging

Diameter of pre-cut, D_i (mm)												
18	19	20	21	22	23	24	25	26	27	28	29	30
x							x	x	0	0	0	

Fig. 21 A comparison of flanges formed by hole-flanging with rotation and conventional hole-flanging experiments
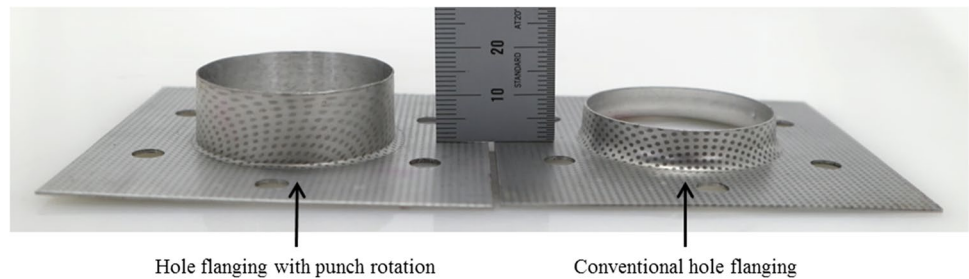
with an HER of 3.3 mm, see Fig. 20. The longest flange lengths were formed at a rotational speed of 4000 rev/min at feeds of 500 mm/min and 1000 mm/min. The flange lengths reduce as the punch speed and feed diverge from these values. The difference in flange length may be explained by the effect of blank temperature on formability and the capacity of the punch to pull the blank at high rotational speeds. There is an increase in blank temperature as punch speed increases from 1000 rev/min to 4000 rev/min which leads to high formability. However, at the high punch speeds (5000 rev/min and 6000 rev/min), friction between the punch and blank reduces as shown by Chowdhury et al. [36]. This decreases the ability of the punch to pull the blank into the die and results in shorter flange lengths. The flange length reduces as the punch feed increases due to a drop in blank temperature and formability. In addition, convex tool geometries with a large edge radius such as the round punch have a lower capacity to pull the blank into the die at high forming feeds and cause

out cracks are represented by zeros (0) in Table 3.

Comparison of stamping with and without punch rotation

The results of experiments on conventional hole-flanging and hole flanging with punch rotation are compared. Figure 21 shows flanges having the maximum HERs made by stamping with punch rotation and conventional stamping.

The forming limits in stamping with punch rotation and conventional hole flanging are compared using the equivalent plastic strains and stress triaxialities of element 1 from the FE simulations in Fig. 8a and Fig. 9a. The magnitudes of the equivalent plastic strains of the inner and outer surfaces of both process variants are almost the same, see Fig. 22a and Fig. 22b. At the beginning of the processes, there is an initial increase in stress triaxiality to about 0.6

Fig. 22 Evolution of stress triaxiality and equivalent plastic strains for flanges with a hole diameter of 10 mm. **a**) Flange formed by conventional hole flanging. **b**) Flange formed by hole-flanging with rotation
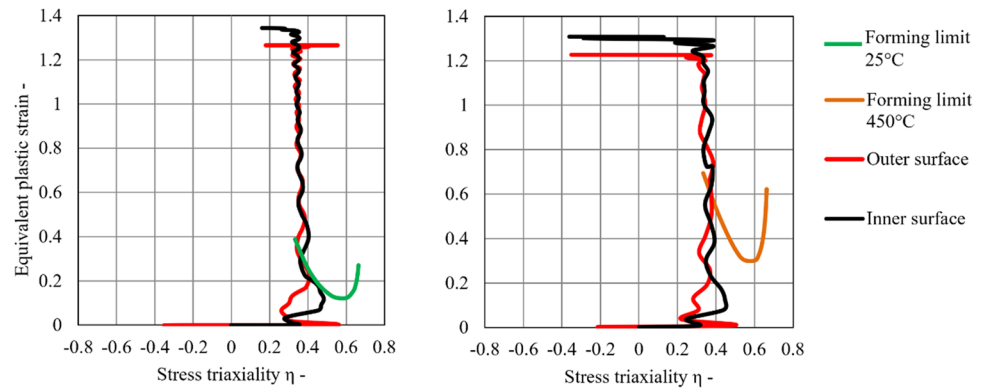
which indicates biaxial stretching. This is followed by a decrease in stress triaxiality to below 0.4, which corresponds to the stress triaxiality in uniaxial tension. There is a wide fluctuation of the stress triaxiality at equivalent plastic strains of 1 and above in stamping with punch rotation (Fig. 22b). This may be caused by stresses due to the spring back of the blank and high-speed punch rotation. The forming limits of the material at the temperatures of the 2 process variants are included in the FLDs. Figure 22a shows a failure of the blank in conventional hole-flanging as expected. This agrees with the results of the hole-flanging tests in Table 3. The forming limit of the conventional hole-flanging process was accurately estimated, in Fig. 13b.

The forming limits obtained from the hot tensile tests fail to estimate the forming limits in stamping with punch rotation because the effects of out-plane stresses-strains and non-proportional loading paths are not included in the plane stress assumption of the M–K model, see Fig. 22b. In addition, there is a high rate of deformation of the blank material in stamping with punch rotation compared to the hot tensile tests, this is demonstrated by the high punch speeds and feeds required. A high rate of deformation enhances formability as demonstrated in Sect. 3.2. Balanethiram et al. [37] showed that strain rates above $15s^{-1}$ cause increased formability using tensile tests and a dramatic rise in formability was observed for very high strains rates (hyperplasticity) in electrohydraulic forming. They further stated that high forming velocities cause the propagation of plastic waves in the blanks. This may change the mechanical properties of the blanks from quasi-static equilibrium to dynamic equilibrium. The change in the constitutive model of the material may increase the forming limits. Neugebauer et al. [38] also stated that high-speed forming causes twinning and strengthening at grain boundaries that increase the load-carrying capacity and formability of blanks.

Besides high strain rates, the round surface of the punch makes a smooth and continuous contact with the blank and induces in-plane shear $\left(\sigma_{12}:\varepsilon_{12}\right)$ and contact stress on the blank that increases formability. The in-plane shear is

included in calculating the membrane stretching and bending energies in Eq. (14). The in-plane shear in stamping with punch rotation can be observed by the slight twist of the grid points from a straight line on the flange surface, as seen in Fig. 21. Shouler and Allwood [39] showed that in-plane shear causes an increase in formability using specially designed tensile test specimens. Similarly, in-plane torsion tests by Traphöner et al. [40] revealed an increase in formability. The increased formability in the presence of shear is because shear stresses-strains may act in planes that prevent void nucleation, crack growth, and coalescence [41]. In-plane shear is absent in tensile tests and low formability was observed in the tensile tests. Non-linear loading of the element indicated by the fluctuation of the strain paths in Fig. 22a enhances the forming limits as demonstrated by Liu et al. [42]. This is due to local compression, varying stress triaxiality and shear, observed by Qian et al. [43]. A recent review on the modeling of forming limits in metal forming by Volk et al. [44] presents the challenges in determining appropriate formability models for different forming processes. The forming limits derived from the hot tensile tests are used to explain the rise in process formability due to punch rotation. However, more extensive tests which involve a range of triaxialities, temperatures and strain rates are required to determine the process forming limit.

Conclusion and outlook

The present research was carried out to increase the formability in axisymmetric hole flanging by using high-speed punch rotation. The maximum HER of stamping with punch rotation was compared with conventional hole-flanging. The following conclusions were made from the investigations.

- Tool rotation leads to a rise in formability. Flanges formed by conventional stamping had an HER of 1.48. However, when the punch was rotated the HER increased

to 4. The gain in formability is due to high forming temperatures and rate of deformation.

- Deformation in both hole-flanging process variants occurs primarily by membrane stretching. Bending constitutes about 10% of the deformation energy. Negligible out-of-plane shear is present as revealed by a split of the plastic energy density from the FE simulations of the processes. Punch rotation reduces the plastic energy density in hole-flanging in stamping with punch rotation due to thermal softening.

- The M–K model reveals that there is an increase in formability due to a rise in blank temperature and strain rate. The process conditions that maximize formability were estimated and the estimated forming conditions agree with the experimental findings.

- The maximum hole expansion of conventional stamping agrees with the estimated forming limit of the material at 25 °C. However, the quantitative forming limit of stamping with punch rotation could not be estimated by the M–K model because of the effects of out of plane stress-strains, non-proportional loading paths, and the difference in the rate of deformation in the tensile tests and hole-flanging with punch rotation. The experimental results showed extended formability of the process. In future, more experiments will be conducted to calibrate better material and formability laws to estimate the forming limit in hole-flanging with punch rotation.

- Optical strain measurements of a flange made at 6000 rev/min speed and 1500 mm/min feed reveal that the principal strains of the flanges formed by stamping with punch rotation are in the left quadrant of the FLD, which is similar to the principal strains obtained in conventional hole flanging.

- The ranges of punch rotational speeds and axial feeds needed to form flanges with no cracks were determined for flanges with HERs of 4 and 3.3. The robustness of the process is shown by the results of the flanges with 3.3 HER. The reliability of the process was demonstrated by temperature measurements from 3 repetitions of flanges having an HER of 2.86 and formed at a punch speed of 6000 rev/min and 500 mm/min feed. The results show that the process temperature is stable and can be controlled to improve formability.

- The flange height is dependent on the punch speed and feed. For flanges with an HER of 3.3, a punch speed of 4000 rev/min and feeds of 500 mm/min and 1000 mm/min formed flanges with the longest length.

- The experiments of hole flanging with punch rotation show that the process is highly suitable for flanging materials with low formability. The punch speed and feed can be controlled to form the blanks at high temperatures and strain rates that achieve the optimum HER for a given material. Forming temperatures of about 450 °C and high strain rates are optimal for EN AW-6181-T1 blanks of 0.8 mm thickness. This corresponds to process parameters approaching a punch speed of 6000 rev/min and a feed of 1500 mm/min. For other materials, the forming temperature can be measured during forming using a thermal sensor and the punch feed and speed adjusted to form flanges using optimum process parameters without the need for time-consuming FE simulations. Thus, the hole flange-ability of other materials can be maximized by using a predefined temperature profile. Hole-flanging with punch rotation increases process formability and opens interesting research into process control and new opportunities for maximizing the HER. The residual stresses of flanges will be analyzed in future works to determine the effects of the forming mechanisms and temperature change which is needed for the take up of the process in industry.

Declaration

Conflict on interests The authors declare that they have no conflict of interest.

References

1. Worswick MJ, Finn MJ. The numerical simulation of stretch flange forming. International Journal of Plasticity. 2000;16 (6):701–720. 8.

2. Suzuki T, Okamura K, Capilla G, Hamasaki H, Yoshida F. Effect of anisotropy evolution on circular and oval hole expansion

behavior of high-strength steel sheets. International Journal of Mechanical Sciences. 2018: 146–147. 556–570.

3. Yoon JI, Jung J, Kim, Jung G, Sohn SS, Lee S, Kim HS. Key factors of stretch-flangeability of sheet materials. J Mater Sci52. 2017; (13):7808–7823.

4. Paul SK. A critical review of hole expansion ratio. Materialia 2019.

5. Centeno G, Silva MB, Cristino VAM, Vallellano C, Martins PAF (2012) Hole-flanging by incremental sheet forming. Int J Mach Tools Manuf 59:46–54

6. Jeswiet J, Geiger M, Engel U, Kleiner M, Schikorra M, Duflou J, Neugebauer R, Bariani P, Bruschi S (2008) Metal forming progress since 2000. CIRP J Manuf Sci Technol 1(1):2–17

7. Groche P, Erhardt R (2004) Lasererwärmung zur Verbesserung des Umformergebnisses beim Kragenziehen von Aluminium- und Magnesiumknetlegierungen. Mater Werkst 35:467–472

8. Motaman SAH, Komerla K, Storms T, Prahl U, Brecher C, Bleck W. Experimental and numerical investigation of dual phase steels formability during laser-assisted hole-flanging. Proceedings of the 21st international Esaform conference on material forming: ESAFORM 2018. Palermo, Italy, 23–25 April 2018: (AIP Conference Proceedings), p. 60005.

9. Yu H, Zheng Q, Wang S, Wang Y (2018) The deformation mechanism of circular hole flanging by magnetic pulse forming. J Mater Process Technol 257:54–64

10 Sow CT, Bazin G, Heuz T, Racineux G (2020) Electromagnetic flanging: from elementary geometries to aeronautical components. Int J Mater Form 13:423–443

11. Duflou JR, Habraken AM, Cao J, Malhotra R, Bambach M, Adams D, Vanhove H, Mohammadi A, Jeswiet J (2017) Single point incremental forming: state-of-the-art and prospects. Int J Mater Form 11(6):743–773

12. Abele E, Liebeck T, Wörn A (2006) Measuring flexibility in investment decision for manufacturing systems. Annals of the CIRP 55(1):433–440

13. Cui Z, Gao L (2010) Studies on hole-flanging process using multistage incremental forming. CIRP J Manuf Sci Technol 2(2):124–128

14. Voswinckel H, Bambach M, Hirt G (2013) Process Limits of Stretch and Shrink Flanging by Incremental Sheet Metal Forming. Key Eng Mater 549:45–52

15. Bambach M, Voswinckel H, Hirt G (2014) A new process design for performing hole-flanging operations by incremental sheet forming. Procedia Engineering 81:2305–2310

16. Borrego M, Morales-Palma D, Martínez-Donaire AJ, Centeno G, Vallellano C (2016) Experimental study of hole-flanging by single-stage incremental sheet forming. J Mater Process Technol 237:320–330

17. Cao T, Lu B, Ou H, Long H, Chen J (2016) Investigation on a new hole-flanging approach by incremental sheet forming through a featured tool. Int J Mach Tools Manuf 110:1–17

18. Laugwitz M, Voswinckel H, Hirt G, Bambach M (2018) Development of tooling concepts to increase geometrical accuracy in high speed incremental hole flanging. Int J Mater Form 11(4):471–477

19. Besong LI, Buhl J, Bambach M (2019) Investigations on hole-flanging by paddle forming and a comparison with single point incremental forming. Int J Mech Sci 164:105143

20. Zhang C, Chu X, Guines D, Leotoing L, Ding J, Zhao G (2014) Effects of temperature and strain rate on the forming limit curves of AA5086 sheet. Proced Eng 81:772–778

21. Allwood JM, Shouler DR. Paddle Forming. A Novel Class of Sheet Metal Forming Processes. CIRP Annals. 2007; 56 (1):257–260.

22. Thiruvarudchelvan S (1984) Hole flanging of sheet metal using rotating and nonrotating punches, West Indian. J Eng, Trinidad, WI 9(2):49–53

23. Geiger M, Merklein M (2007) Sheet metal forming – a new kind of forge for the future. Key Eng Mater 344:9–20

24. Oliver X. Agelet de Saracibar C. Continuum mechanics for engineers theory and problems. 2nd edition, March 2017 https://doi.org/10.13140/RG.2.2.25821.20961.

25. Maqbool F, Bambach M (2018) Dominant deformation mechanisms in single point incremental forming (SPIF) and their effect on geometrical accuracy. Int J Mech Sci 136:279–292

26. Fatemi A, Dariani B (2015) Forming limit prediction of anisotropic material subjected to normal and through thickness shear stresses using a modified M– K model. Int J Adv Manuf Technol 80:1497–1509

27. Keeler SP, Backofen WA (1963) Plastic instability and fracture in sheets stretched over rigid punches. Trans ASM 56:25–48

28. Marciniak Z, Kuczynski K (1967) Limit strains in the processes of stretch forming sheet steel. J Mech Phys Solids 1:609–620

29. ABAQUS. ABAQUS analysis user's manual [M]. Vélizy- Villacoublay: Dassault Systems, 2012.

30. Allwood JM. Towards CNC metal forming processes. NorthWestern University. Tuesday 17 February 2009: JMA NorthWestern Feb 2009 v5 – CiteSeerX.

31. Khamei AA, Dehghani K (2015) Hot Ductility of Severe Plastic Deformed AA6061 Aluminum Alloy. Acta Metall Sin 28(3):322–330

32. Martinez Domaire AJ, Borrego M, Morales-Palma D, Centeno G, Vallellano C (2019) Analysis of the influence of stress triaxiality on formability of hole-flanging by single-stage SPIF. Int J Mech Sci 151:76–84

33. Chung K, Ma N, Park T, Kim D, Yoo D, Kim C (2011) A modified damage model for advanced high strength steel sheets. Int J Plast 27:1485–1511

34. Borrego M, Morales-Palma D, Martínez-Donaire AJ, Centeno G, Vallellano C. Analysis of formability in conventional hole flanging of AA7075-O sheets: punch edge radius effect and limitations of the FLC. Int J Mater Form 2019.

35. Besong LI, Buhl J, Bambach M (2019) Paddle shape optimization for hole-flanging by paddle forming through the use of a predefined strain path in finite element analysis. J Machine Eng 19(2):83–98

36. Chowdhury MA, Khalil MK, Nuruzzaman DM, Rahaman ML. The effect of sliding speed and normal load on friction and wear property of aluminium. International Journal of Mechanical & Mechatronics Engineering IJMME-IJENS Vol: 11 No: 01.

37. Balanethiram VS, Hu X, Altynova M, Daehn GS (1994) Hyperplasticity: Enhanced Formability at High Rates. J Mater Process Technol 45:595–600

38. Neugebauer R, Bouzakis K, Denkena B, Klocke F, Sterzing A, Tekkaya AE, Wertheim R. Velocity Effects in Metal Forming and Machining Processes. CIRP Annals—Manufacturing Technology, 60 (1) (2011), pp. 627–650.

39. Shouler DR, Allwood JM (2010) Design and use of a novel sample design for formability testing in pure shear. J Mater Process Technol 210:1304–1313

40. Traphöner H, Heibel S, Clausmeyer T, Tekkaya AE (2018) Influence of manufacturing processes on material characterization with the grooved in-plane torsion test. Int J Mech Sci 146–147:544–555

41. Allwood JM, Shouler DR (2009) Generalised forming limit diagrams showing increased forming limits with non-planar stress states. Int J Plast 25(7):1207–1230

42. Liu W, Lian J, Münstermann S, Zeng C, Fang X (2020) Prediction of crack formation in the progressive folding of square tubes during dynamic axial crushing. Int J Mech Sci 176:105534

43. Qian L, Ji W, Sun C, Fang G, Lian J (2021) Prediction of edge fracture during hole-flanging of advanced high-strength steel considering blanking pre-damage. Eng Fracture Mechanics 248:107721

44. Volk W, Groche P, Brosius A, Ghotti A, Kinsey BL, Liewald M, Madej L, Min J, Yanagimoto J (2019) Models and modelling for process limits in metal forming. CIRP Ann 68(2):775–798